

Supporting Information

A Co(III)-peptoid complex as a fast electrocatalyst for homogeneous water oxidation with low overpotential

*Guilin Ruan^a, Lee Engelberg^a, Pritam Ghosh^a, and Galia Maayan^{*a}*

Schulich Faculty of Chemistry, Technion-Israel Institute of Technology, Technion
City, Haifa 3200008, Israel. E-mail address: gm92@technion.ac.il.

Experimental Procedures

Materials

Rink Amide resin was purchased from Novabiochem; benzylamine and ethanolamine were purchased from Acros organics, Israel; N,N'-diisopropylcarbodiimide (DIC), bromoacetic acid were purchased from Sigma Aldrich; 4'-Chloro-2,2':6',2''-terpyridine and TFA were purchased from Alfa Aesar. The purchased reagents, solvents, and HPLC grade reagents were purchased from commercial sources and used without further purification, except for DMF that was dried with molecular sieves.

2-(2,2':6,2''-terpyridine-4'-yloxy)ethylamine was synthesized by a previously published procedure.¹ Protection of -OH group of ethanolamine was done by a reported procedure.² The used solvents were HPLC grade. High purity deionized water was obtained by passing distilled water through a nanopore Milli-Q water purification system. Aqueous buffer solutions (pH range 8-10) were prepared using specific concentrations of mono, di- and tribasic phosphate salts with added 0.1 M NaOH solution such that the final ionic strength was 0.1 M (monitored by pH meter).

Synthesis of complex TPT₂Co:

The peptoid TPT (1M in MeOH) was treated with 1 molar equivalent of cobalt acetate tetrahydrate (Co(CH₃COO)₂ • 4H₂O) in MeOH was added and the mixture was allowed to stir for 2 hours. The formed complex was precipitated using excess sodium perchlorate (NaClO₄, 1M in MeOH) and centrifuged for 10 minutes. Then the excess solution was removed. The solid complex was purified by washing with cold MeOH (2 ml × 5-6 times) until the solvent became colorless. The metal complexes were analyzed by ESI-MS, UV-Vis spectroscopy, ¹H-NMR, EPR, and FTIR.

Instrumentation

All peptoids were analyzed by reverse-phase HPLC (analytical C18(2) column, Phenomenex, Luna 5μm, 100 Å, 2.0x50 mm) on a Jasco UV-2075 PLUS detector. A linear gradient of 5–95% acetonitrile (MeCN) in water (0.1% TFA) over 10 mins was

used at a flow rate of 0.7 mL/min. Preparative HPLC was performed using an AXIA Packed C18(2) column (Phenomenex, Luna 15 μ m, 100 Å, 21.20x100mm). Peaks were eluted with a linear gradient of 5–95% MeCN in water (0.1% TFA) over 60 mins at a flow rate of 5 mL/min. Mass spectrometry of peptoid oligomer and metallopeptoid was performed on an Advion expression CMS mass spectrometer, under electrospray ionization (ESI), direct probe MeCN:H₂O (95:5), flow rate 0.2 mL/min. High-resolution mass spectrometry for metallopeptoid was performed on a Maxis Impact Bruker Q-TOF mass and Advion expression mass under electrospray ionization (ESI), direct probe MeCN: H₂O (70:30), flow rate 0.5 ml/min. UV-Vis measurements were performed using an Agilent Cary 60 UV-Vis spectrophotometer, a double beam, Czerny-Turner monochromator, 1 cm quartz cuvette. EPR spectra were obtained on a Bruker EMX-10/12 X-band ($\nu = 9.2$ GHz) digital EPR spectrometer equipped with a Bruker N₂ temperature controller. Samples were irradiated with the focused and filtered ($\lambda = 300$ nm) light of a high-pressure mercury lamp (1 kW) (ARC lamp power supply model 69920) in the resonator of EPR spectrometer. All spectra were recorded at a non-saturating microwave power of 200 mW, 100 kHz magnetic field modulation of 1 G amplitude. Spectra processing and simulation were performed with a Bruker WIN-EPR and SimFonia Software. The g-factors values were determined using 2,2,6,6- tetramethylpiperidine-N-oxyl (TEMPO) as reference ($g = 2.0058$). Scanning electron microscopic (SEM) images were taken from the TESCAN VEGAII Nanospace instrument. FTIR spectra (400-4000 cm⁻¹) were recorded on an "Agilent Cary 630" FTIR spectrometer, equipped with a diamond attenuated total reflection (ATR) instrument, which allows direct measurement. The ¹H-NMR spectra were recorded on a Bruker 400 MHz instrument. Coupling constants are given in Hz.

Electrochemical Methods

Electrochemical studies were measured at RT using 563 Model "IVIUMSTAT.XRe" potentiostat/galvanostat. Each complex was initially characterized by Cyclic Voltammetry (CV) to detect catalytic activity and to

understand the working potential; later, controlled potential electrolysis (CPE) experiments were done to quantify the catalytic activity: determine the turn over number (TON), turn over frequency (TOF) and to calculate the Faradic efficiency (FE%). The CVs were carried out by placing solutions of complexes in one-compartment 3-electrode cells. Glassy Carbon (GC) was used as a working electrode (0.07 cm^2) unless mentioned specifically otherwise, Ag/AgCl as a reference electrode and Pt wire as a counter electrode. Working electrode pretreatment before each measurement included polishing with $0.05 \text{ }\mu\text{m}$ alumina paste following by rinsing with water and acetone and finally drying in air. All redox potentials in the present work are reported versus NHE by adding 0.20 V to the measured potential. CVs were collected at 100 mV/s unless specified otherwise. When measuring CVs in organic solvent acetonitrile was used, tetrabutylammonium hexafluorophosphate ($[\text{NBu}_4]\text{PF}_6$) was added in a concentration of 0.1 M to act as a supporting electrolyte, and Ag/AgNO₃ used as a reference electrode instead of Ag/AgCl electrode.

Controlled Potential Electrolysis

Experiments were performed in a two-compartment "H-cell" separated by a medium-porosity sintered glass frit. Three-electrode assembly was used consisting of: vitreous carbon as the working electrode, Pt wire as the counter (auxiliary) electrode, and an Ag/AgCl/3M KCl reference electrode ($+0.2 \text{ V vs. NHE}$). A Half-cell of WE and the reference electrode was loaded with the catalyst (0.5 mM concentration). 10 atm. of Argon/N₂ was bubbled before the experiment to purge the oxygen, measurements began as soon as the oxygen level was stable. The system was well sealed using septum, parafilm, and plasticine and stirred continuously with a magnet.

The Faradaic efficiency (FE%) of the process can be determined in bulk electrolysis experiment: by comparing the actual amount of oxygen evolved during bulk electrolysis (as indicated by the direct measurement of oxygen using the oxygen sensor), and the charge accumulated over this period, using the eqn. S4 & S5.

Oxygen Sensor

Oxygen evolution was monitored in the gas phase with a Fixed Needle-Type Oxygen Minisensor (from PyroScience) placed in the headspace of the reaction vassal (working electrode side). The CPE started as soon as the oxygen sensor signal was stable. During the experiment, solutions of both compartments were vigorously stirred. The results of the water oxidation catalysis with Co complex compared with the blank experiment in the same conditions but in the absence of the catalyst. The Faraday efficiency was determined according to the total charge passed during the CPE and the total amount of generated oxygen as a four-electron oxidation process. The oxygen was measured by the oxygen sensor in % and converted to μmol using a calibration curve (Fig. S34). This was constructed by the gradual addition of the known amount of pure oxygen (μL) into the cell containing buffer solution using a Hamilton syringe while measuring the oxygen in % by the oxygen sensor and then by plotting the amount of pure oxygen added (μL) vs. the amount of oxygen (%) shown by oxygen sensor to get the total amount of oxygen evolved in μL during electrolysis. This was further converted to μmol via the equation: $y \mu\text{mol} = x \mu\text{L}/(24.5 \text{ L/mol})$, $T = 298 \text{ K}$.

Supplementary Figures

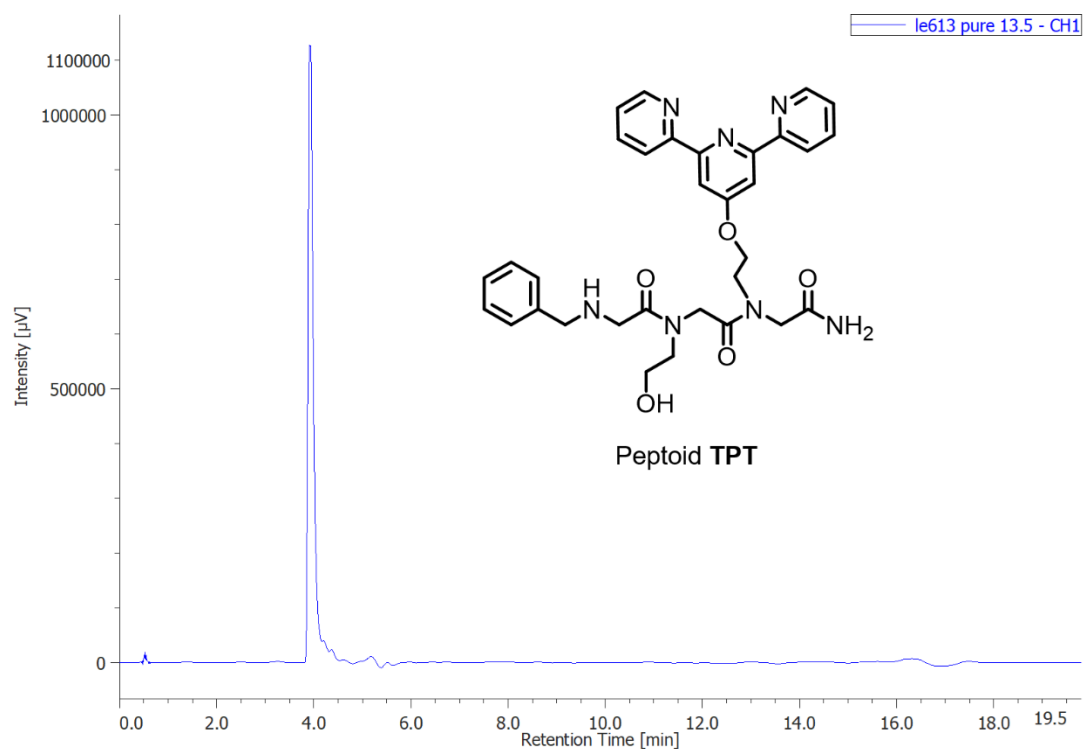


Figure S1. Analytical HPLC trace of pure peptoid **TPT**.

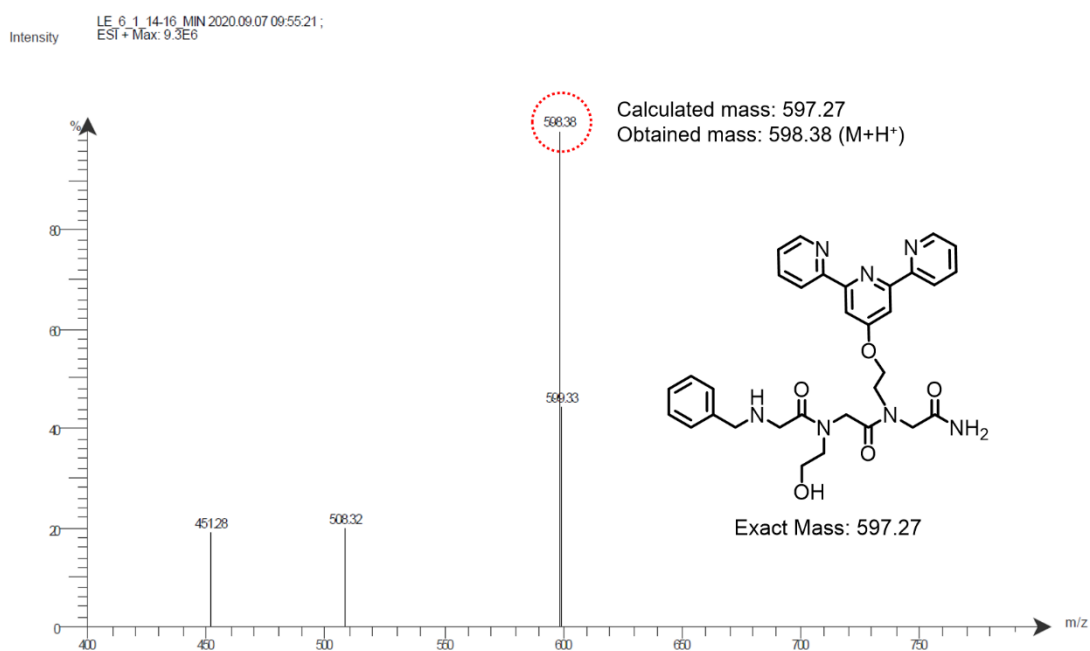


Figure S2. ESI-MS of peptoid **TPT** in water.

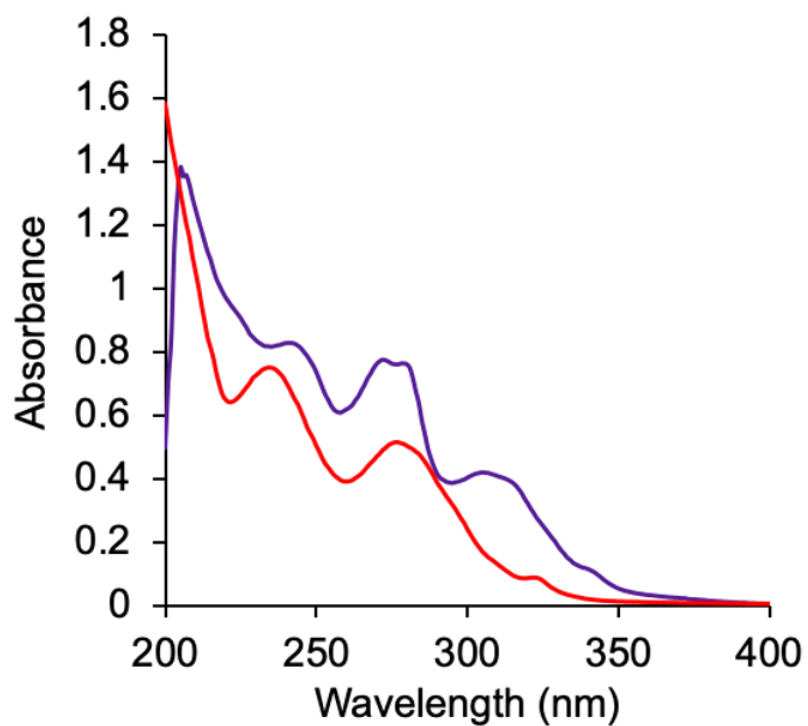


Figure S3. UV-Vis spectra of 49 μM of the peptoid **TPT** (red line) and complex **TPT₂Co** (blue line) in water.

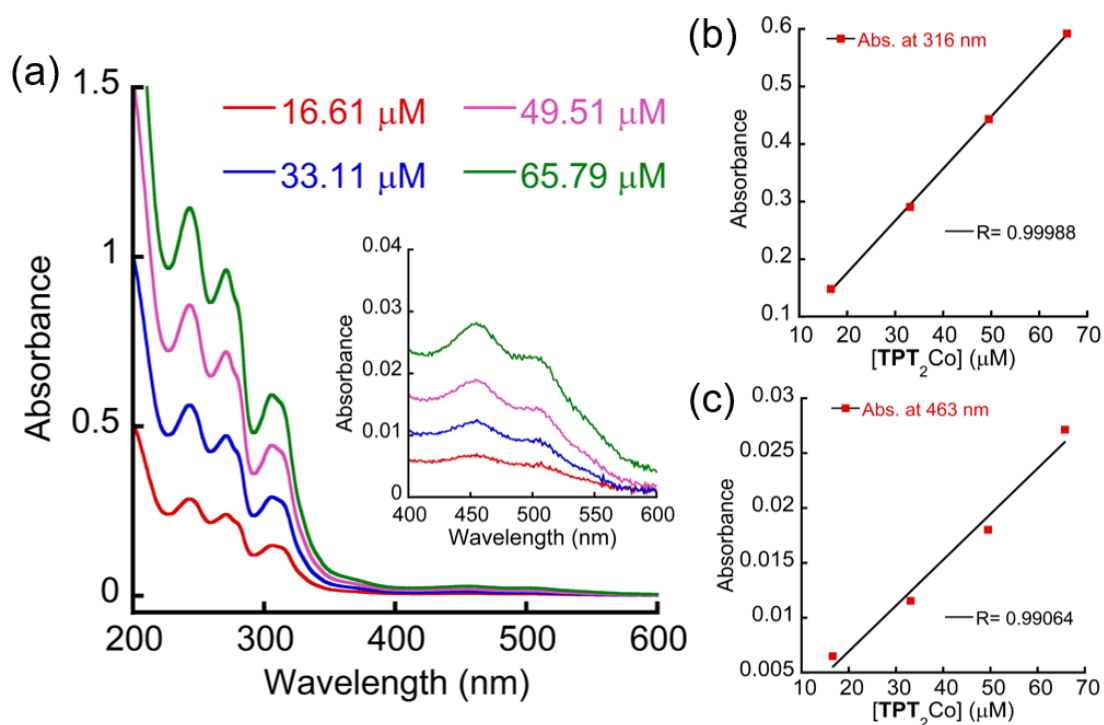


Figure S4. (a) UV-Vis spectra of complex TPT_2Co with different concentrations in water. (b) Linear plot of absorbance vs. concentration of TPT_2Co at 316 nm. (c) Linear plot of absorbance vs. concentration of TPT_2Co at 463 nm.

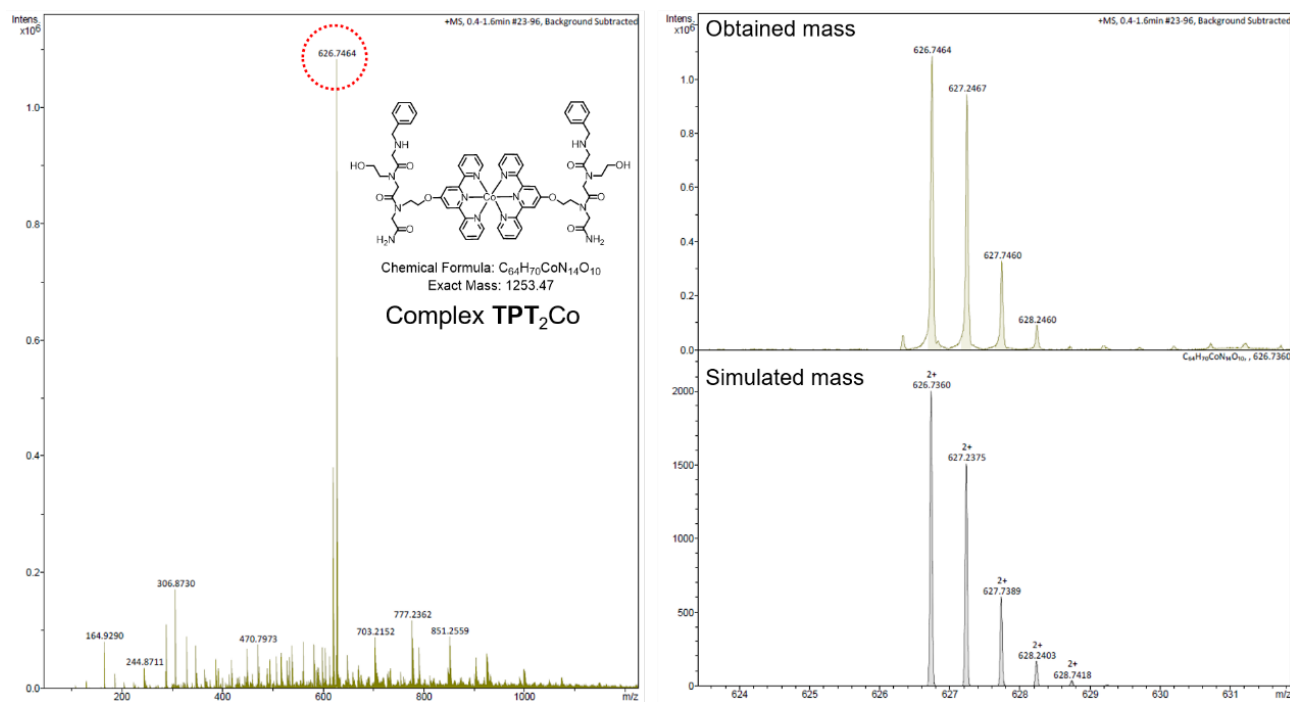


Figure S5. High-resolution ESI-MS of complex TPT_2Co in water.

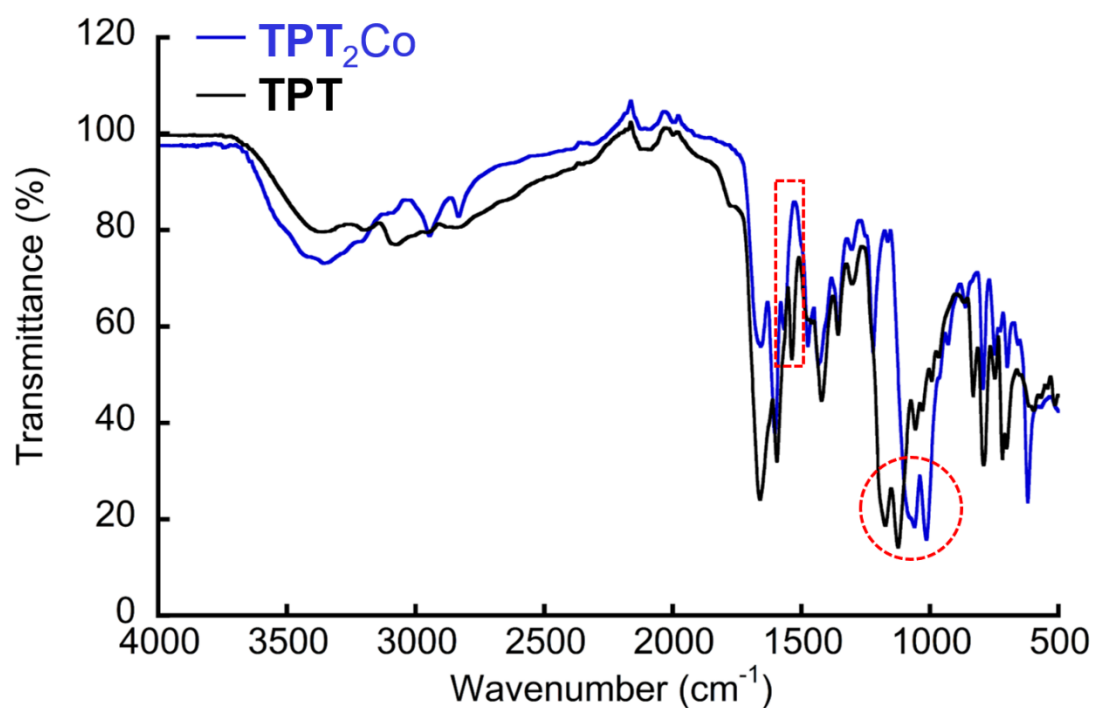


Figure S6. FTIR spectra of the solid peptoid **TPT** and complex **TPT₂Co**. *The red dash circle indicates the C-N stretching shift (1125 to 1177 and 1013 to 1062 cm⁻¹, respectively), and the red dash square indicates the C=N stretching shift (1539 to 1561 cm⁻¹, respectively).

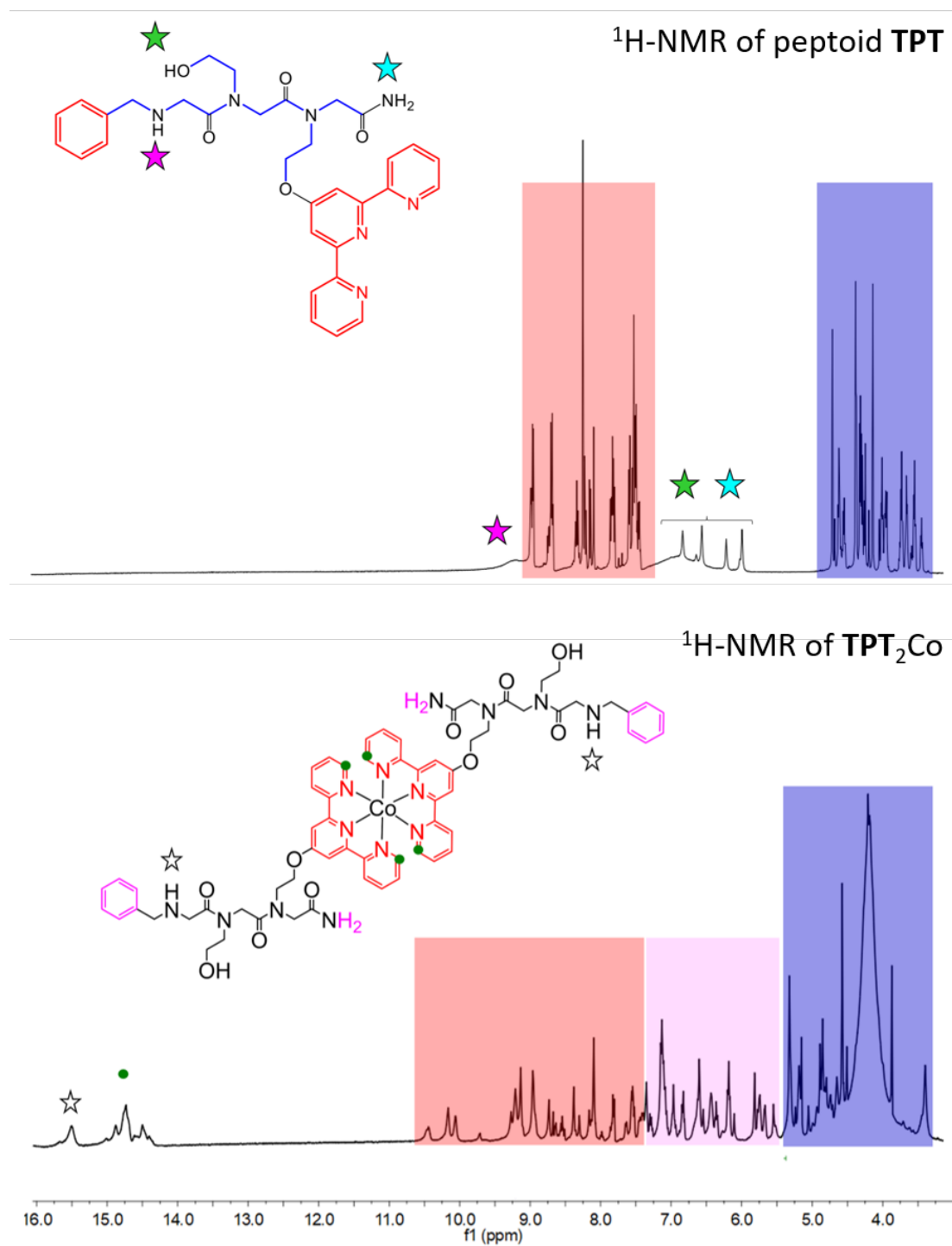


Figure S7. $^1\text{H-NMR}$ of peptoid **TPT** (top) and complex **TPT**₂Co (bottom) in a mixture of deuterated water and acetonitrile.

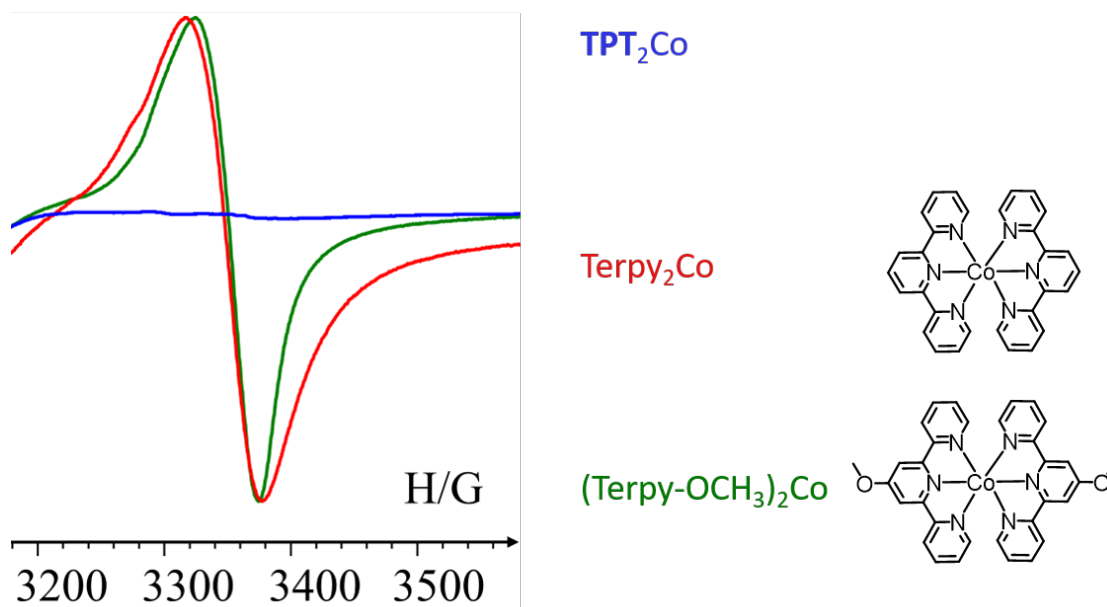


Figure S8. EPR spectrum of complex TPT_2Co (blue line), Terpy_2Co (red line), and $(\text{Terpy-OCH}_3)_2\text{Co}$ (green line). *The results of Terpy_2Co and $\text{Terpy-OCH}_3)_2\text{Co}$ are consistent to typical of $S = 1/2$ $(\text{Terpy}_2\text{Co})^{2+}$ -type center.^{3,4} The comparison strongly points to the conclusion that Co ion is stable at Co(III) oxidation low-spin state. If it is Co(II) or Co(III) high-spin state, which is paramagnetic, the EPR spectrum is not silent.

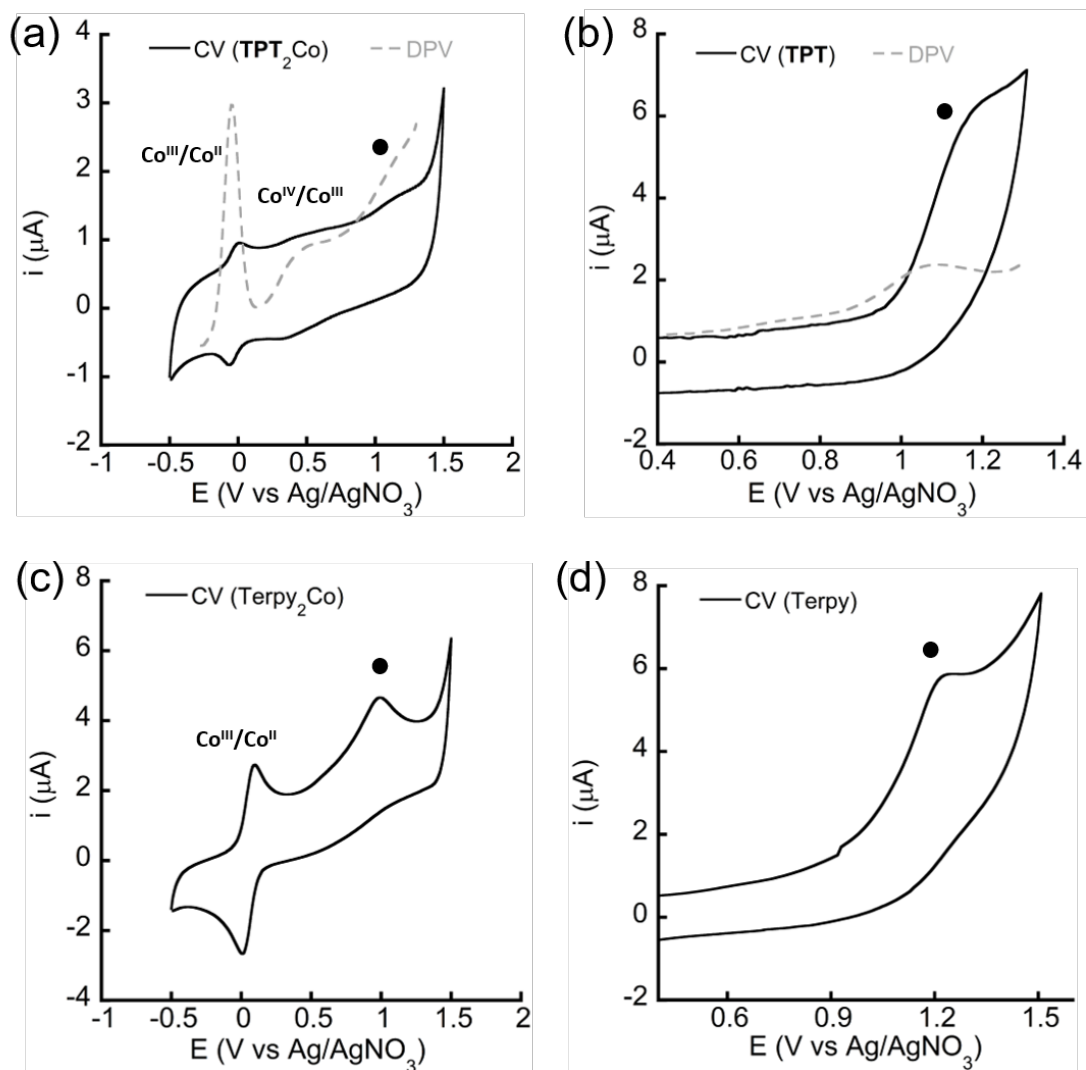


Figure S9. (a) CV and DPV of 0.5 mM TPT_2Co in acetonitrile; (b) CV and DPV of ~ 1 mM of peptoid ligand **TPT** in acetonitrile; (c) CV of ~ 1 mM Terpy_2Co in acetonitrile; (d) CV of ~ 1 mM ligand (Terpy) terpyridine in acetonitrile. All the experiments were performed with glassy carbon as working electrode, Ag/AgNO_3 (0.01M AgNO_3 , 0.1M TBAP in acetonitrile) as reference electrode, Pt wire as counter electrode, scan rate = 100 mV/s.

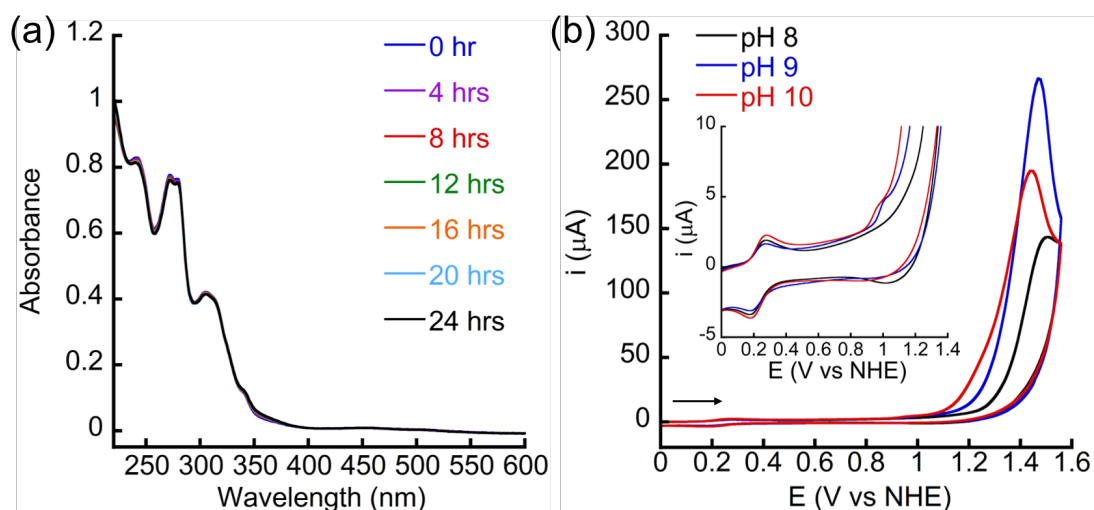


Figure S10. (a) UV-Vis absorption of 49 μM TPT_2Co in 0.1 M phosphate buffer solution at pH 9; (b) CVs of 0.5 mM TPT_2Co in 0.1M phosphate buffer at pH 8, 9, and 10 at scan rate 100 mV/s with a glassy carbon working electrode (0.07 cm^2).

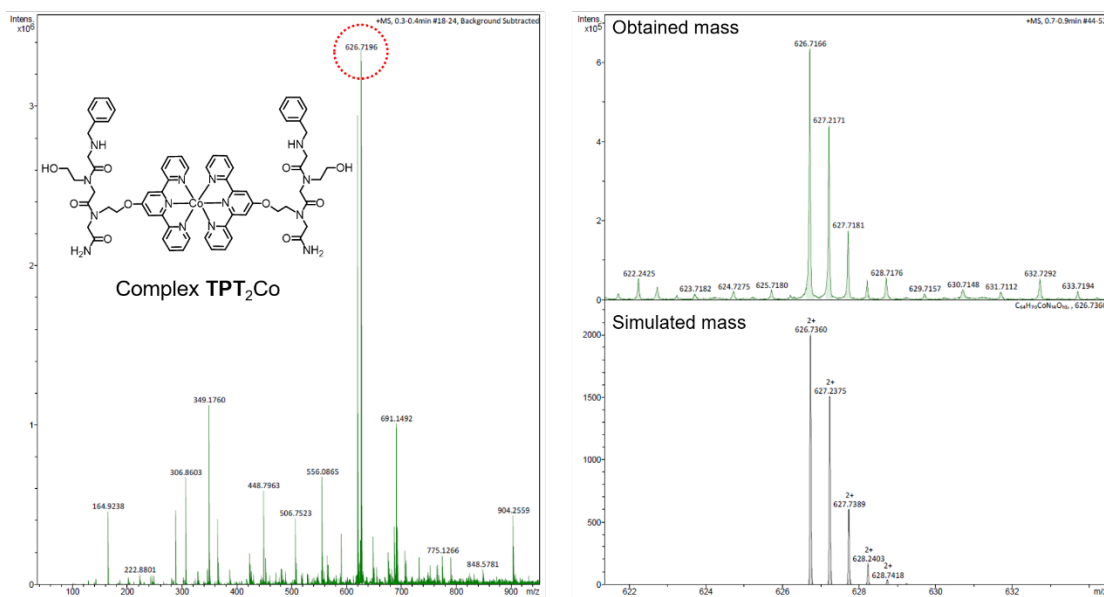


Figure S11. High-resolution ESI-MS of complex TPT_2Co in 0.1M phosphate buffer at pH 9.0.

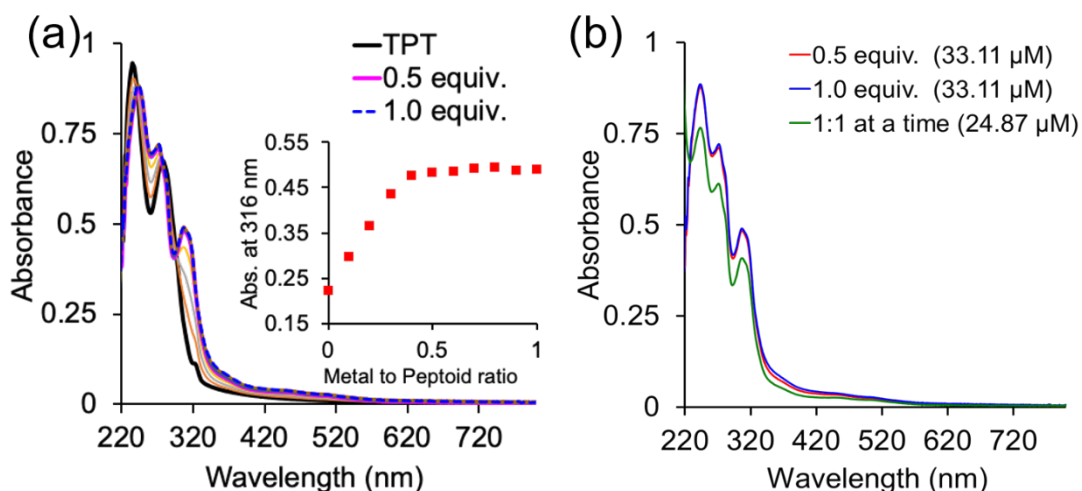


Figure S12. (a) UV-Vis spectra and (insert) metal-to-peptoid ratio plot for the titration of peptoid **TPT** with Co ion in 0.1M phosphate buffer solution at pH 9.0. The peptoid (33.11 μM) was titrated with Co ion dissolved in water in multiple steps. (b) A clear UV-Vis spectra comparison of 1.0 equiv. of peptoid with 0.5 (red), 1.0 (blue) equiv. of Co ion after titration extracted from (a) and with 1.0 (green) of Co ion added at one time with fixed concentration. **These experiments clearly show identical absorption bands and intensities after the ratio of metal-to-peptoid up to 0.5:1.0, indicating that 1 Co ion coordinates to 2 peptoids and becomes saturated once this species fully formed.*

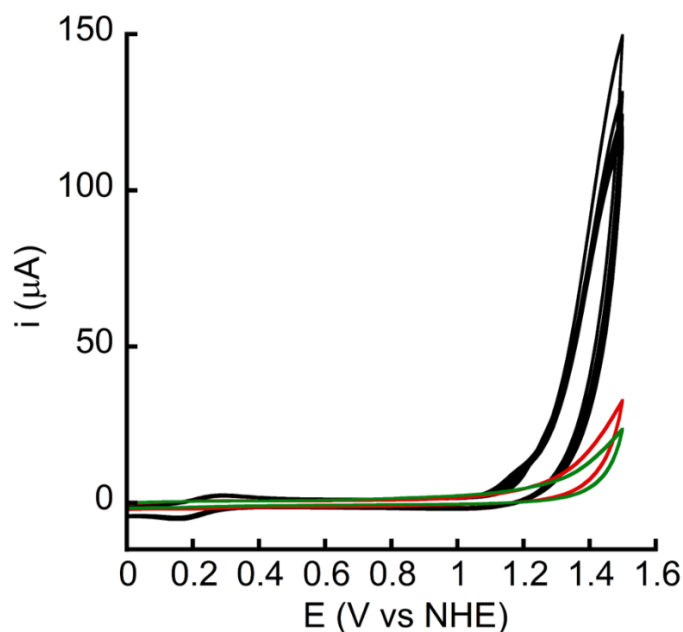


Figure S13. Homogeneity test of the electrode surface.⁵ This figure depicts a CV with a clean glassy carbon working electrode (0.07 cm^2) buffer solution without catalyst (green line), 20-continued CVs (blank lines), and the CV response (red line) of the working electrode in a blank 0.1 M phosphate buffer.

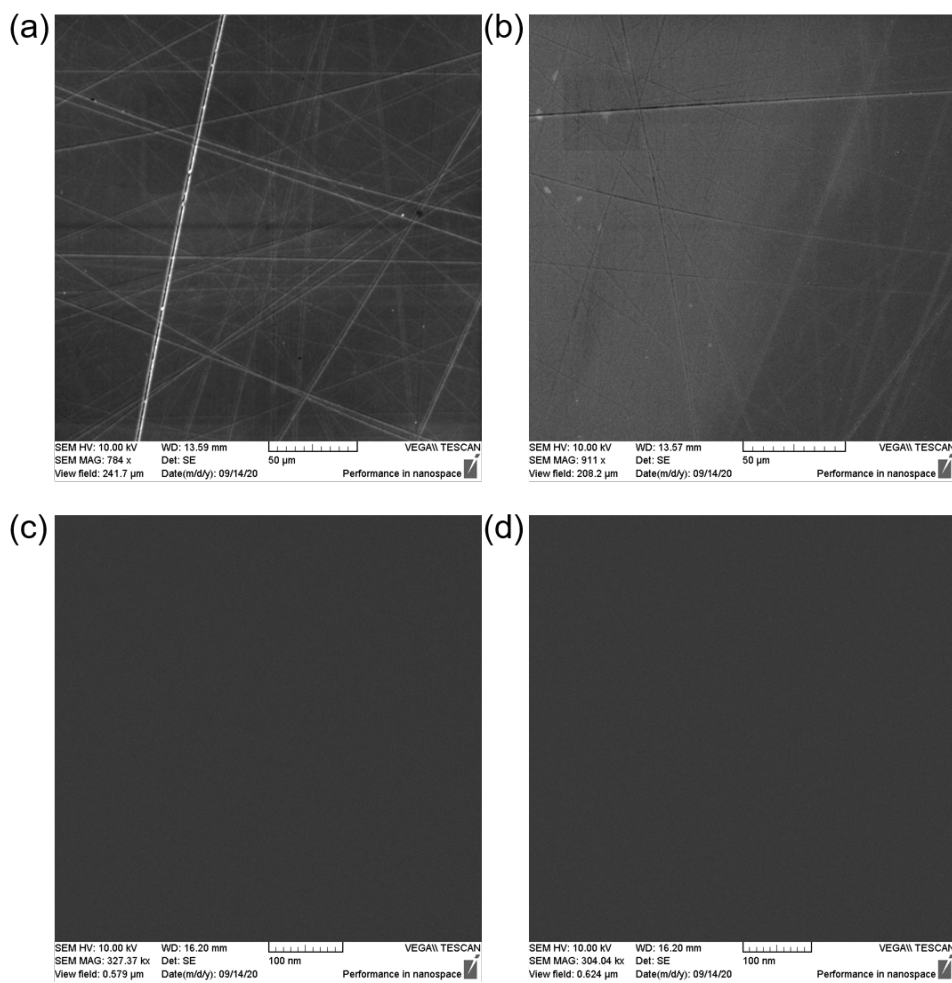


Figure S14. SEM images of the glassy carbon electrode before (a)(c) and after (b)(d) continuous 20 CV scans measured in different scales.

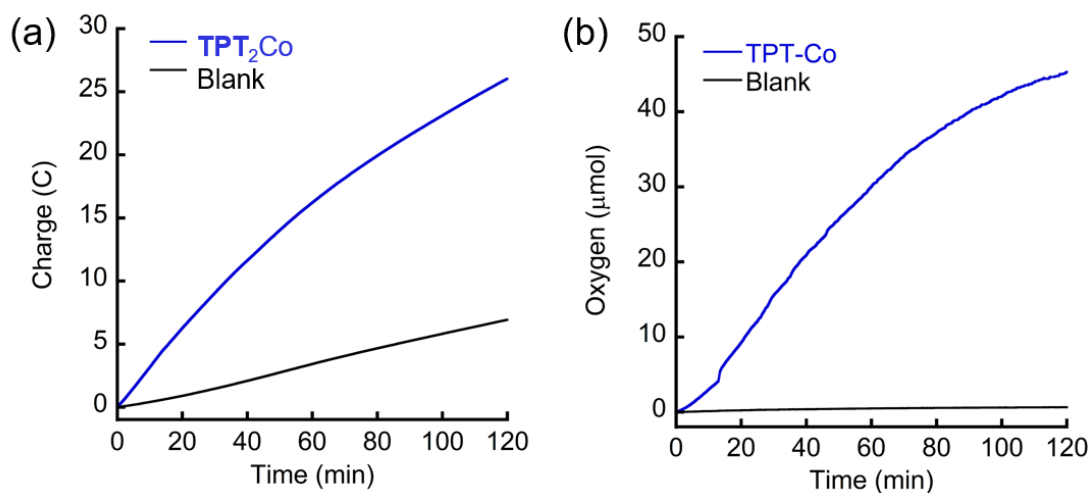


Figure S15. Total accumulated charge during control potential electrolysis from a solution containing 0.5 mM catalyst **TPT**₂Co and the buffer only using a porous GC at +1.45 V vs. NHE for 2 hours in 0.1M phosphate buffer solution at pH 9.

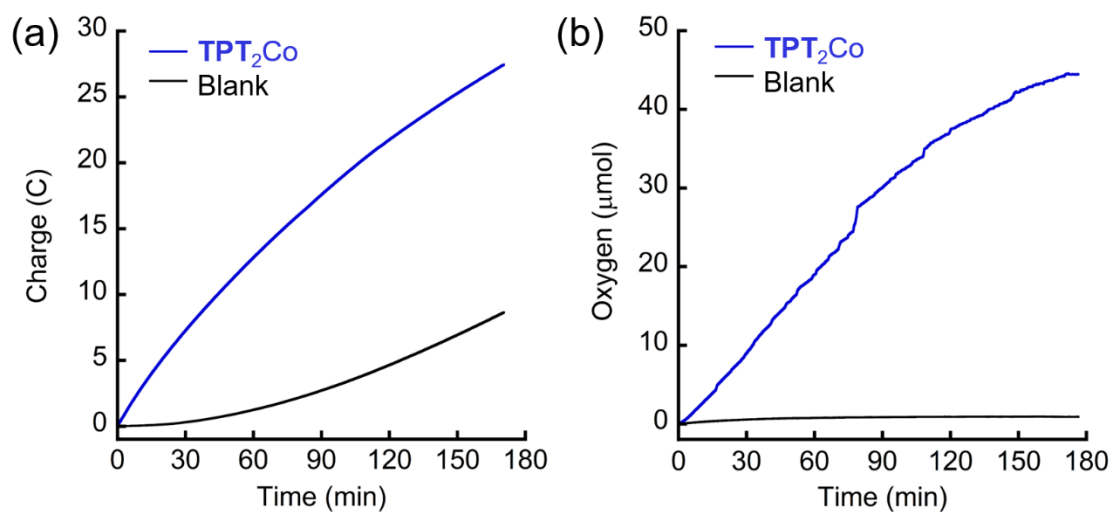


Figure S16. (a) Total accumulated charge during control potential electrolysis from a solution containing 0.5 mM catalyst **TPT**₂Co and the buffer only using a porous GC at +1.35 V vs. NHE for about 3 hours. (b) The evolution of O₂ during electrolysis was measured with a fluorescence probe. All solutions contained 0.1 M phosphate buffer at pH 9.0.

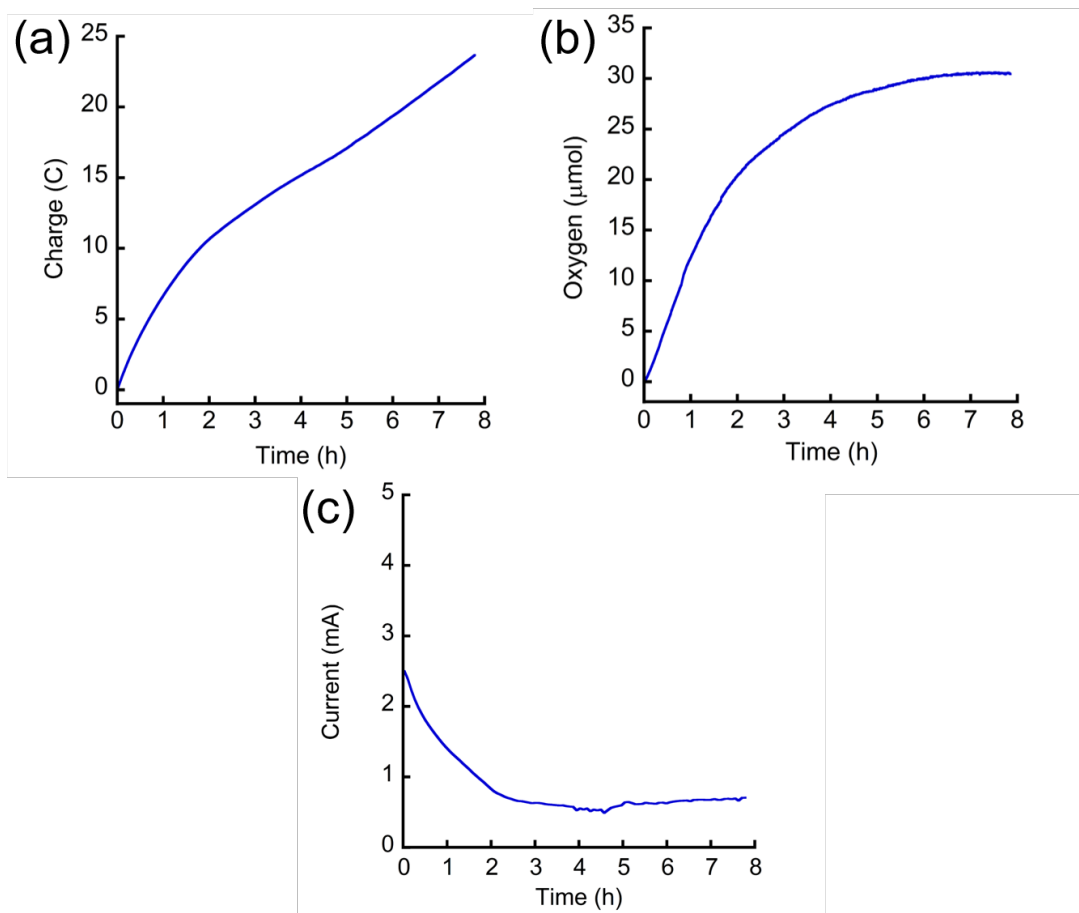


Figure S17. (a) Total accumulated charge during control potential electrolysis from a solution containing 0.5 mM catalyst TPT_2Co and the buffer only using a porous GC at +1.25 V vs. NHE for 8 hours. (b) The evolution of O_2 during electrolysis was measured with a fluorescence probe. (c) The total current passed during the 10-hour experiment. All solutions contained 0.1 M phosphate buffer at pH 9.0. **The oxygen evolution is non-linear along with time and almost became plateau after approximately 5-hour electrolysis. We suggest that the catalytic activity of TPT_2Co decreases with the pH drop during the CPE experiment.*

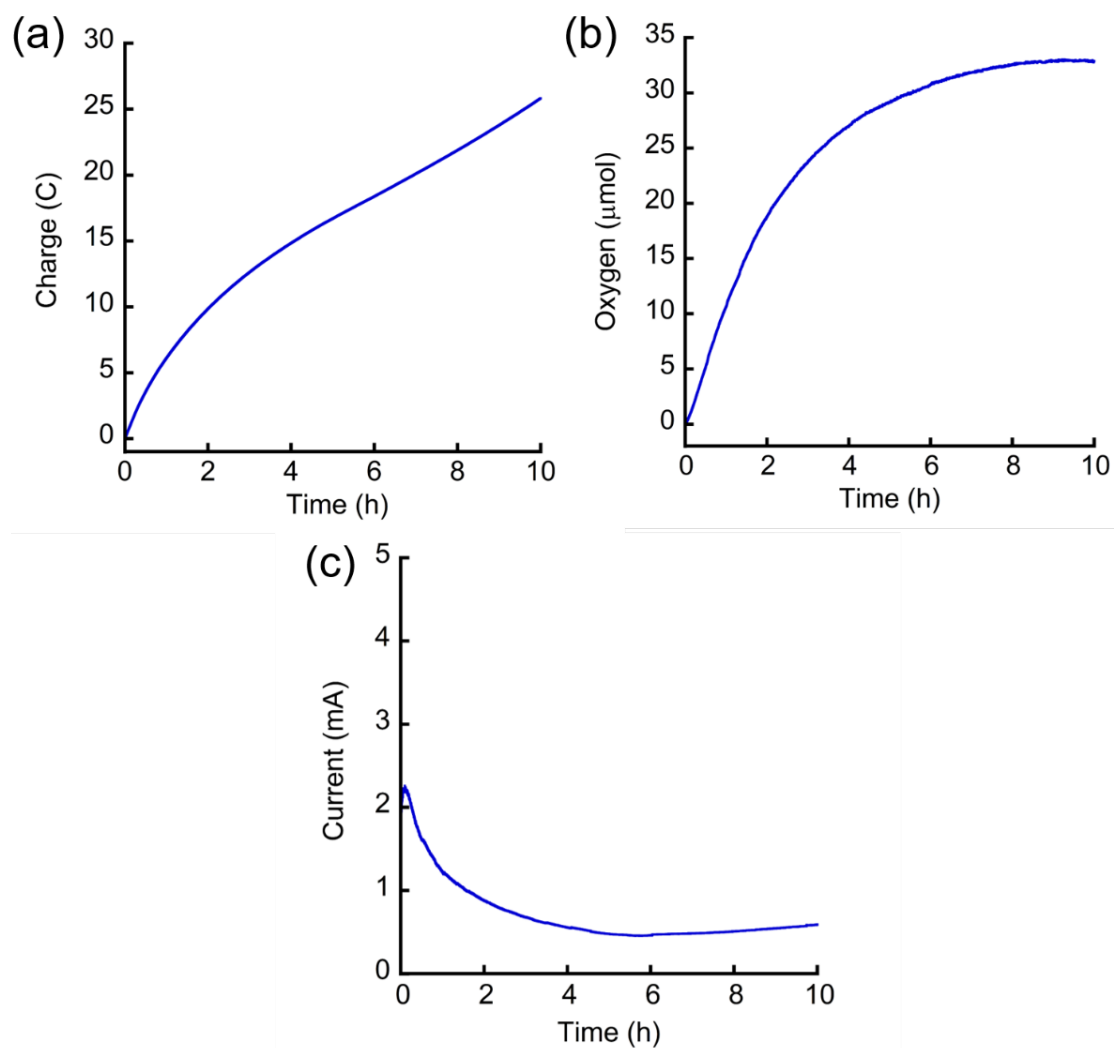


Figure S18. (a) Total accumulated charge during control potential electrolysis from a solution containing 0.5 mM catalyst TPT_2Co and the buffer only using a porous GC at +1.20 V vs. NHE for 10 hours. (b) The evolution of O_2 during electrolysis was measured with a fluorescence probe. (c) The total current passed during the 10-hour experiment. All solutions contained 0.1 M phosphate buffer at pH 9.0. **The oxygen evolution is non-linear along with time and almost became plateau after approximately 7-hour electrolysis. We suggest that the catalytic activity of TPT_2Co decreases with the pH drop during the CPE experiment.*

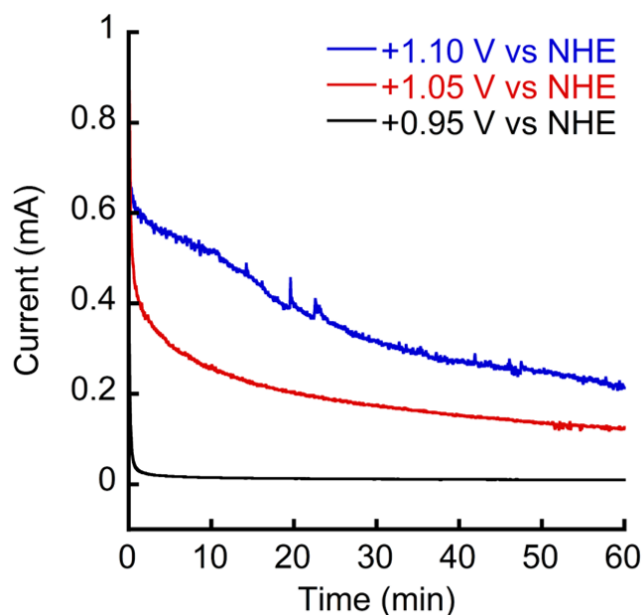


Figure S19. The total current passed during control potential electrolysis for 60 minutes of a solution of 0.5 mM TPT_2Co with different applied potentials. All solutions contained 0.1M phosphate buffer at pH 9.0.

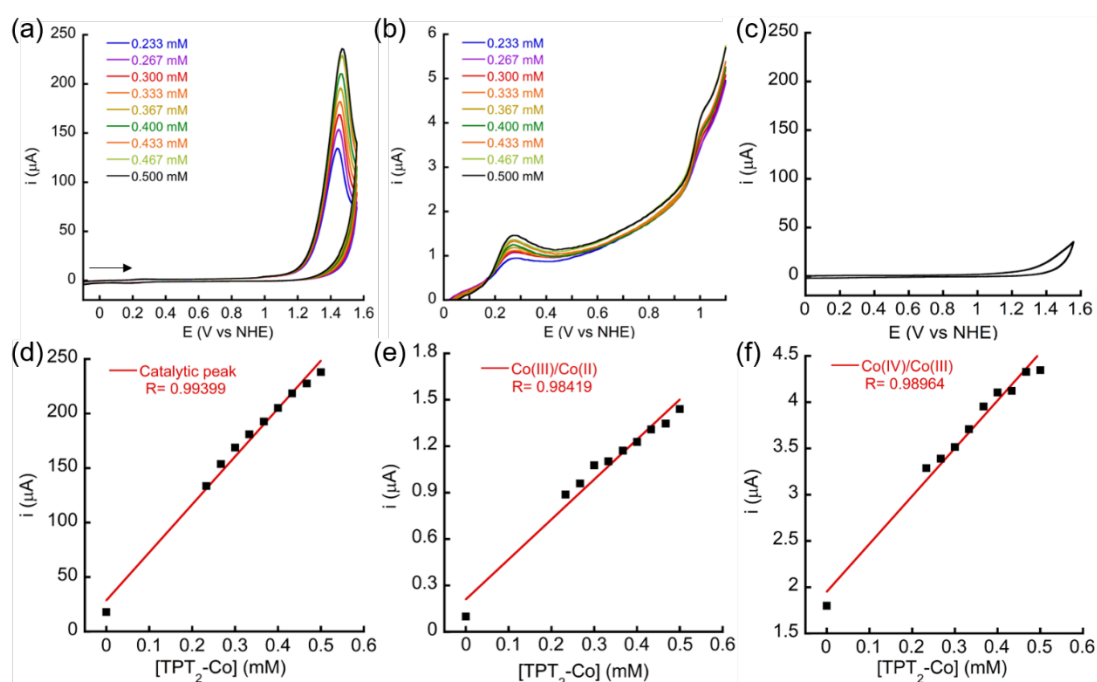


Figure S20. (a) CVs of different concentrations of TPT_2Co in 0.1 M phosphate buffer solution at pH 9.0. (b) Enlarged scale of (a) to clearly show the $\text{Co}^{\text{III/II}}$ and $\text{Co}^{\text{IV/III}}$ oxidation waves. (c) Blank CV at pH 9 to extract data as 0 mM of catalyst. (d): Linear regression of i_{cat} vs catalyst concentration. (e) Linear regression of $i_{\text{Co}^{\text{III/II}}}$ vs catalyst concentration. (f) Linear regression of $i_{\text{Co}^{\text{IV/III}}}$ vs. catalyst concentration.

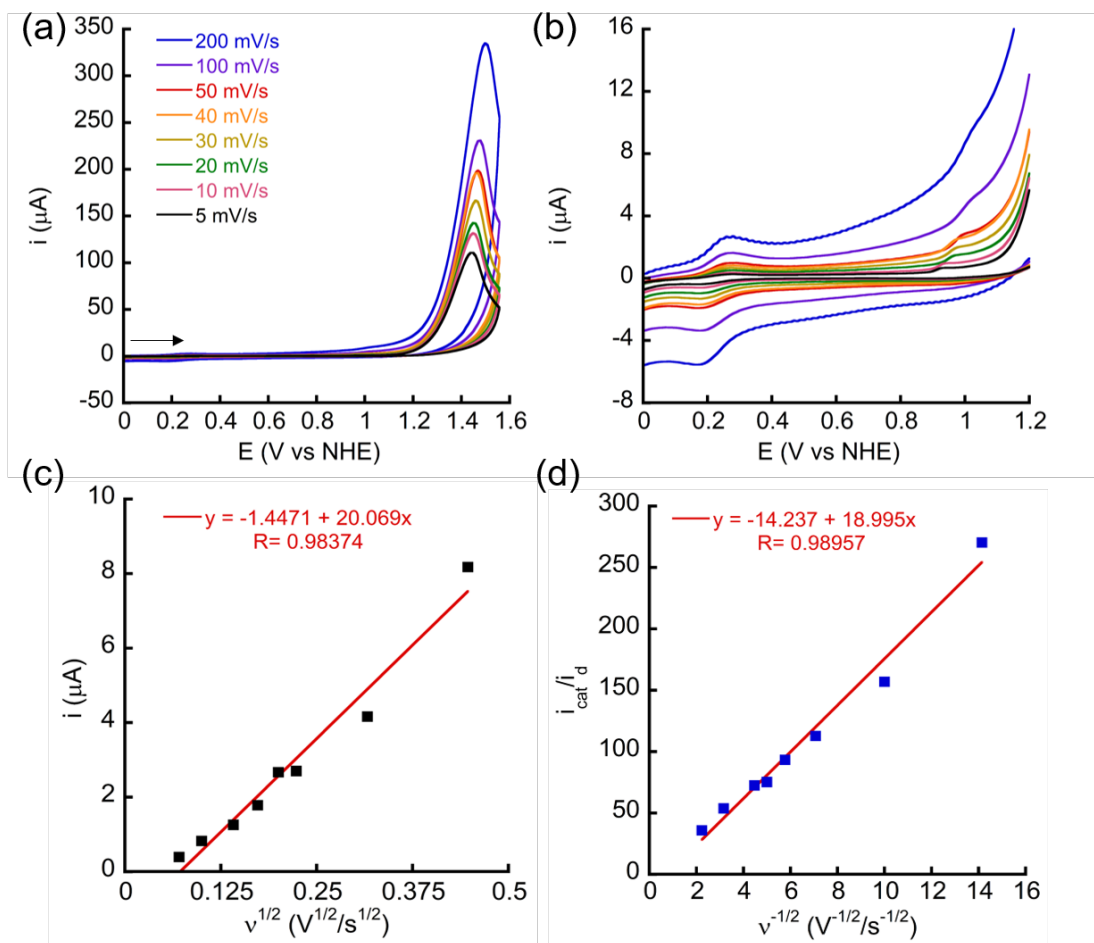


Figure S21. (a) CVs of $0.5 \text{ mM TPT}_2\text{Co}$ solution with different scan rates on a glassy carbon electrode in 0.1 M phosphate buffer at pH 9.0. (b) Enlarged scale of (a) to clearly show $\text{Co}^{\text{III/II}}$ and $\text{Co}^{\text{IV/III}}$ oxidation waves. (c) The $\text{Co}^{\text{IV/III}}$ is plotted against the square root of the scan rate (v). (d) The $i_{\text{cat}}/i_{\text{d}}$ is plotted against the $v^{-1/2}$.

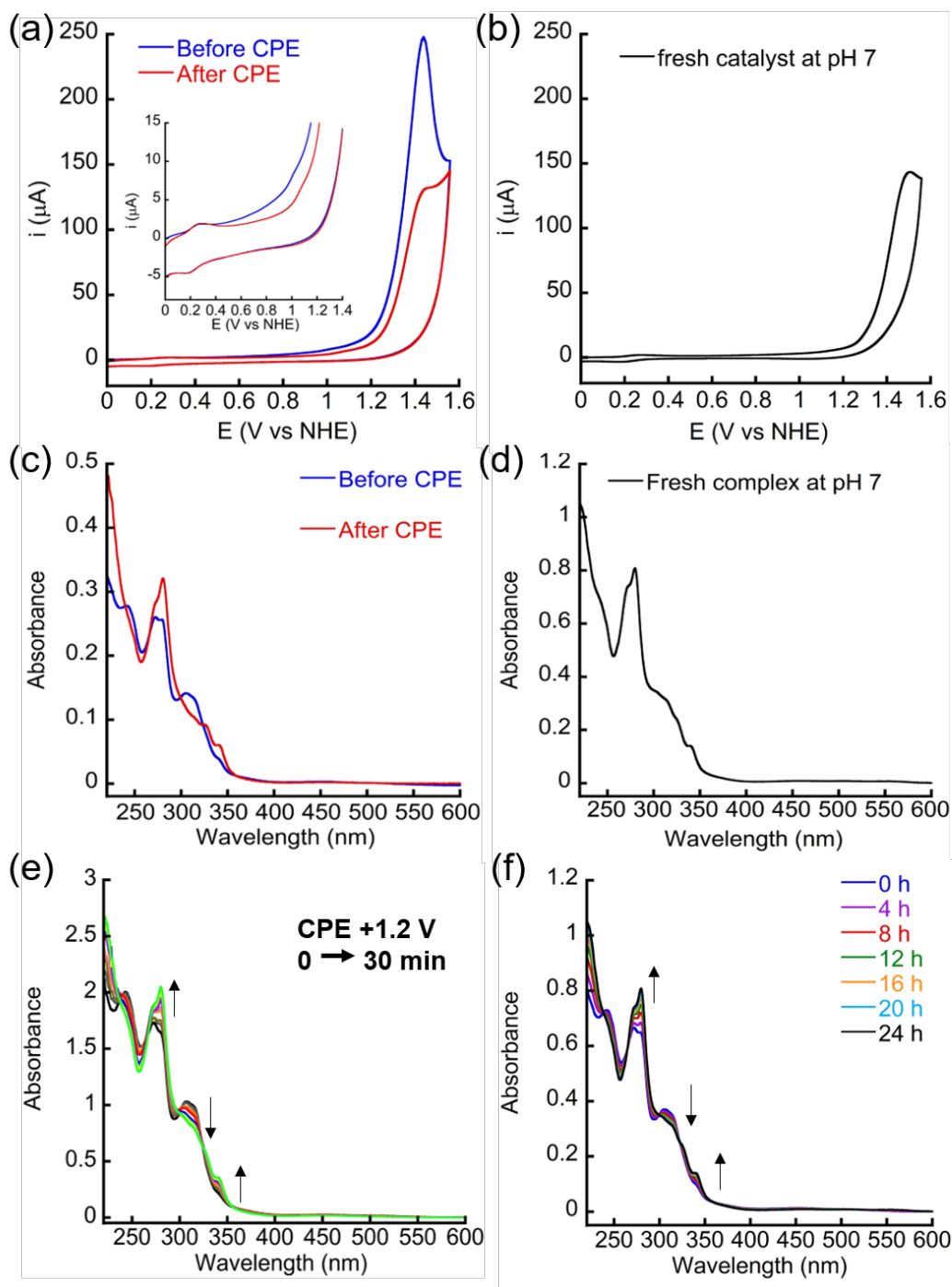


Figure S22. (a) CVs of the complex TPT_2Co in 0.1M phosphate buffer solution at pH = 9.0 before and after 3-hour CPE experiment with +1.20 V applied potential; (b) CV of fresh complex TPT_2Co in 0.1M phosphate buffer solution at pH = 7.0; (c) UV-Vis absorption of TPT_2Co before and after 3-hour CPE experiment with +1.20 V applied potential, data is extracted from Fig. 4a; (d) UV of fresh complex TPT_2Co in 0.1M phosphate buffer solution after 24 hours at pH = 7.0; (e) UV-Vis absorption of TPT_2Co in every 3 minutes during CPE experiment in phosphate buffer pH 9.0 with +1.20 V vs. NHE applied potential; (f) UV-Vis absorption of TPT_2Co in phosphate buffer pH 7 without disturbing for 24 hours.

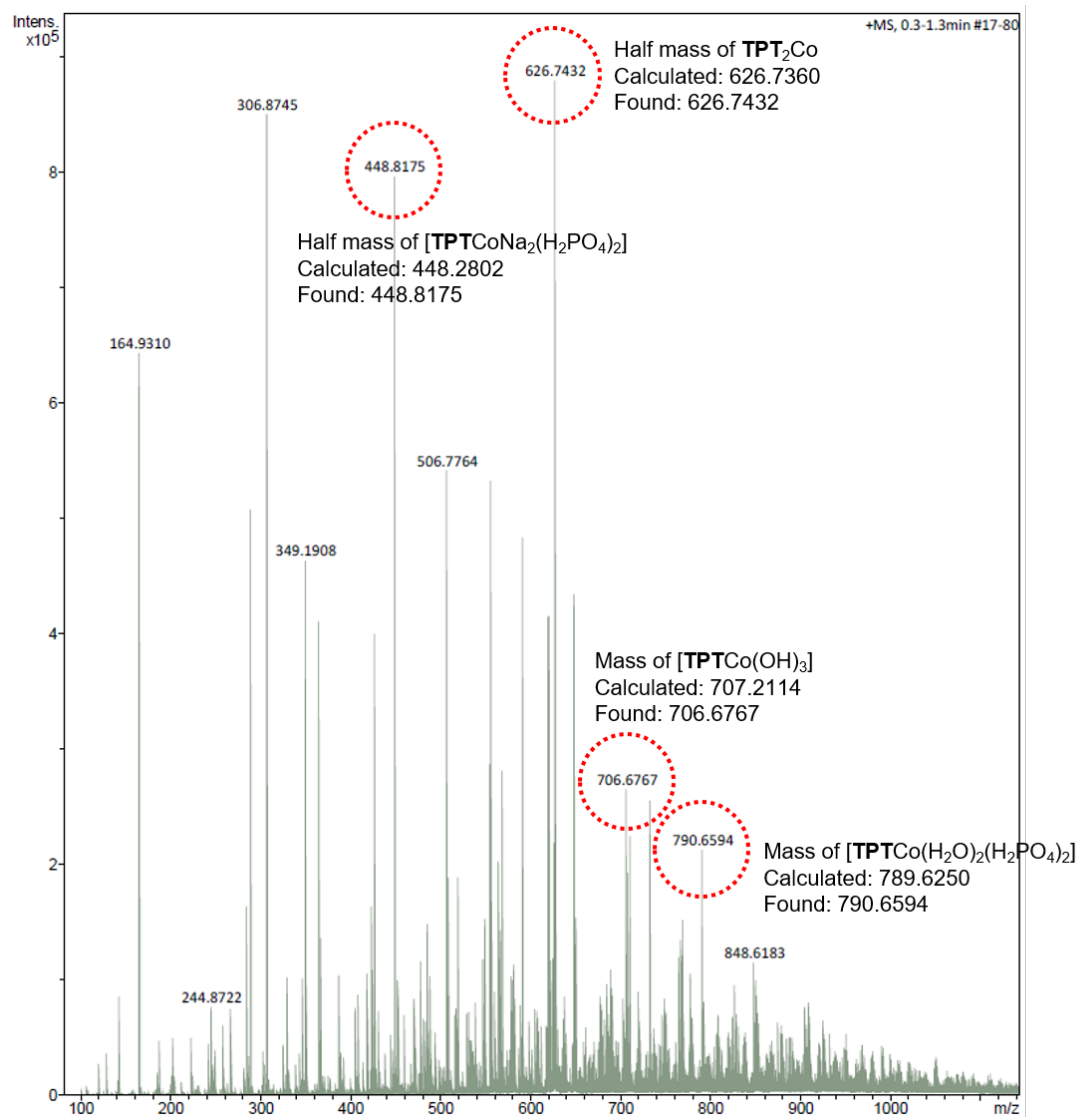


Figure S23. ESI-MS of the catalytic solution after 3 hours CPE at 1.2 V, pH 9.

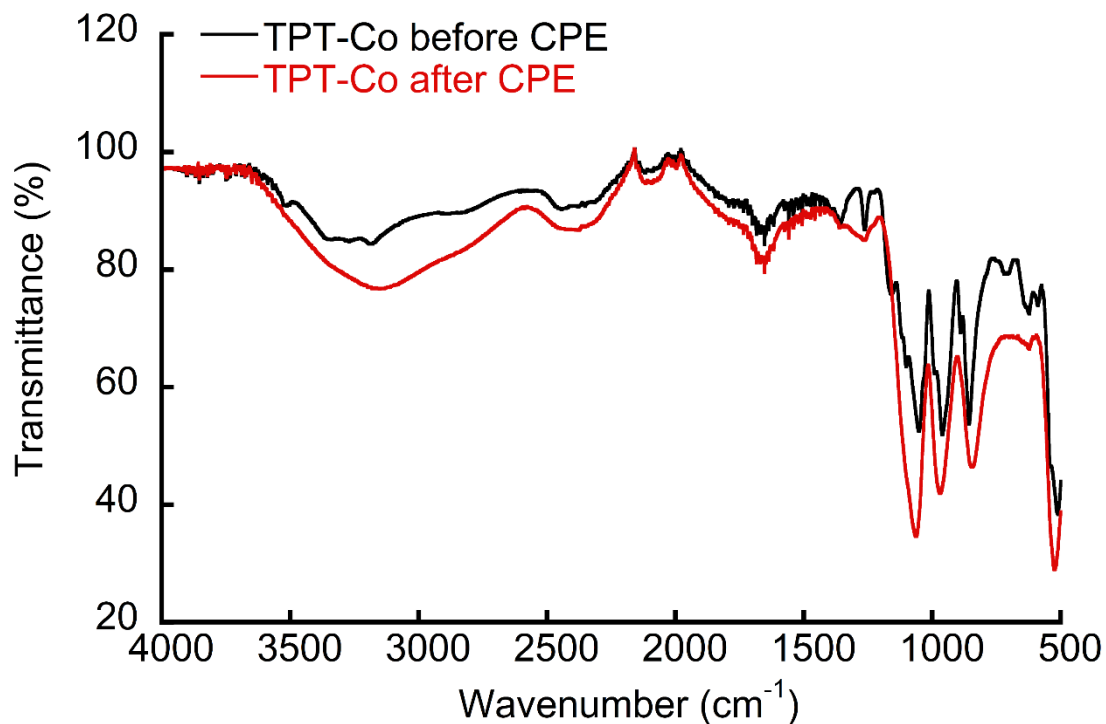


Figure S24. FTIR of the dried solid complex TPT_2Co before and after a 3-hour CPE experiment with +1.20 V applied potential.

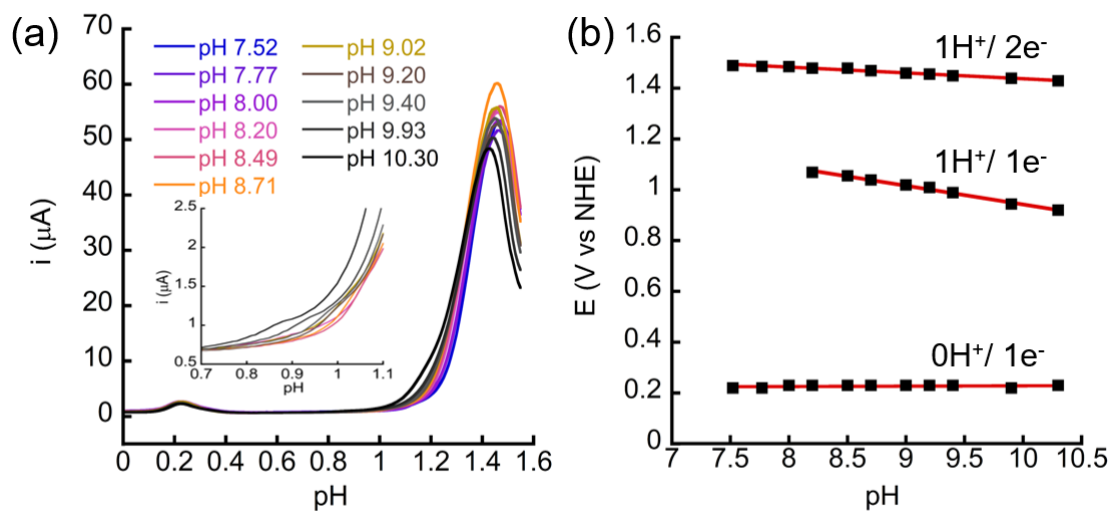


Figure S25. (a) DPVs and (b) Pourbaix diagram of TPT_2Co in phosphate buffer at pH range between 7.52 to 10.30.

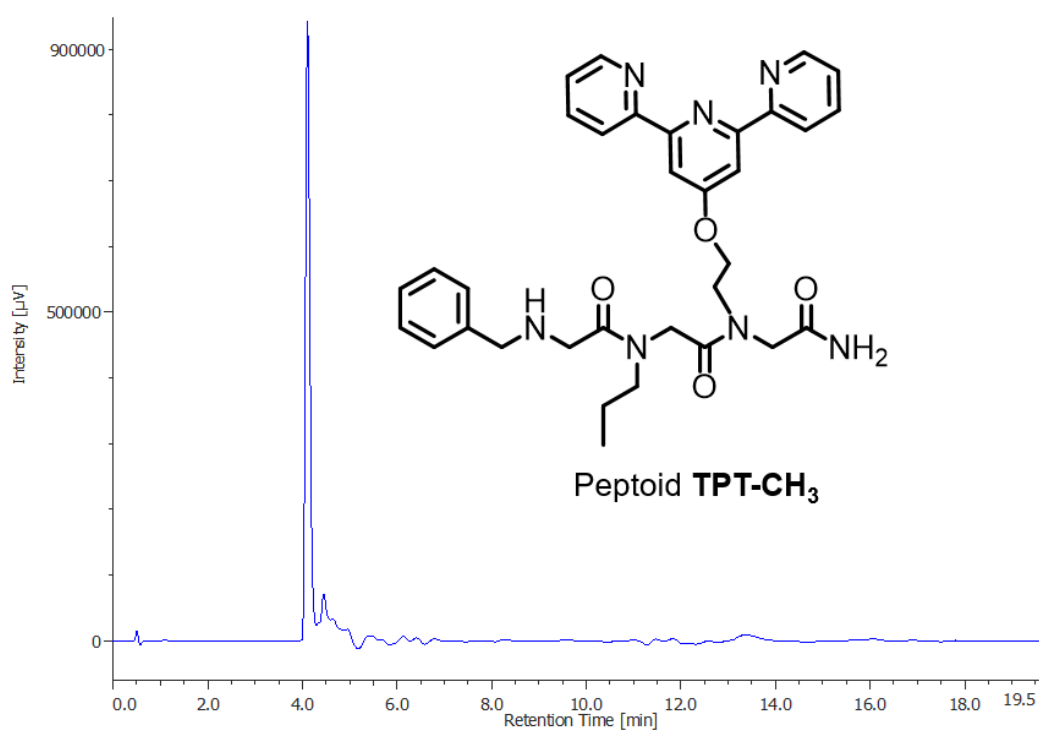


Figure S26. Analytical HPLC trace of pure peptoid **TPT-CH₃**.

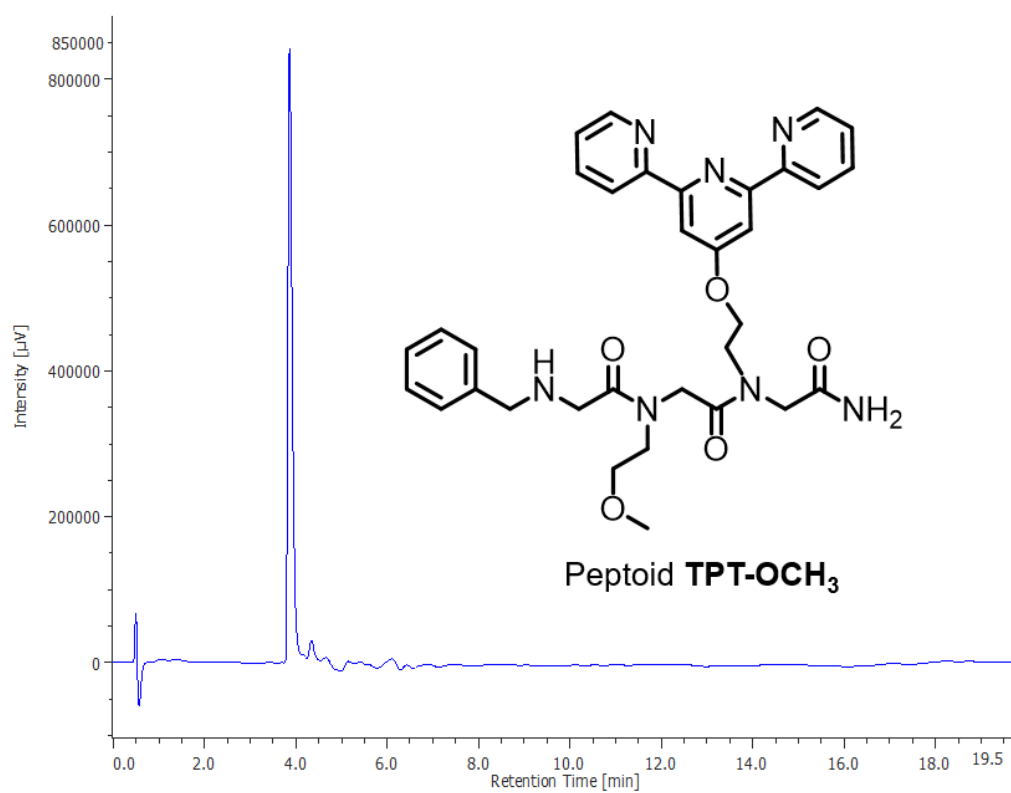


Figure S27. Analytical HPLC trace of pure peptoid **TPT-OCH₃**.

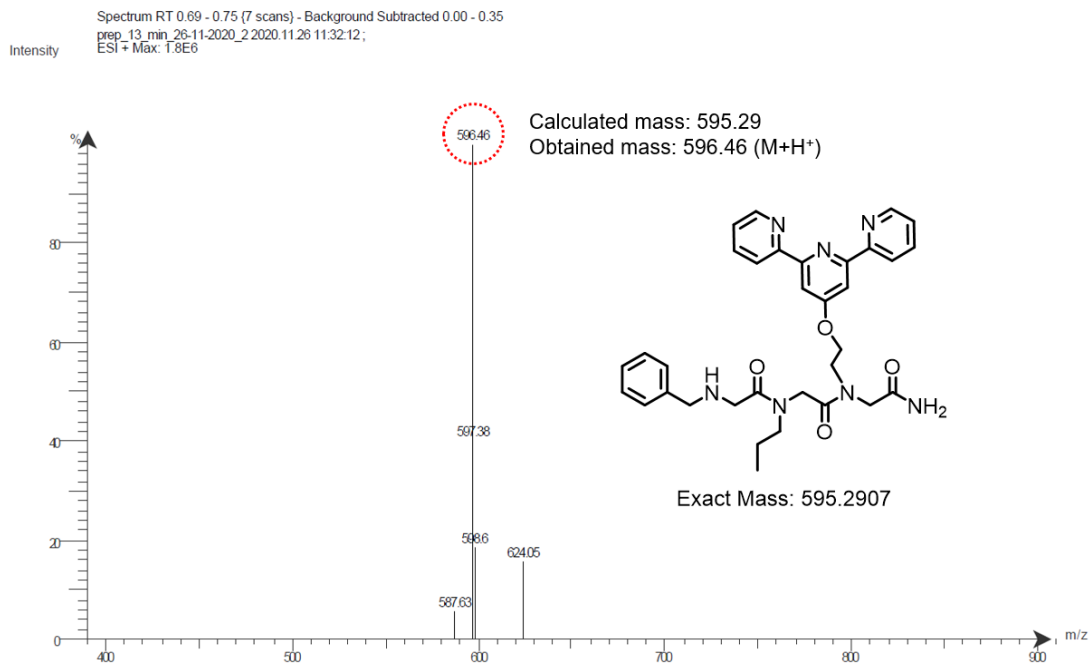


Figure S28. ESI-MS of peptoid **TPT-CH₃** in water.

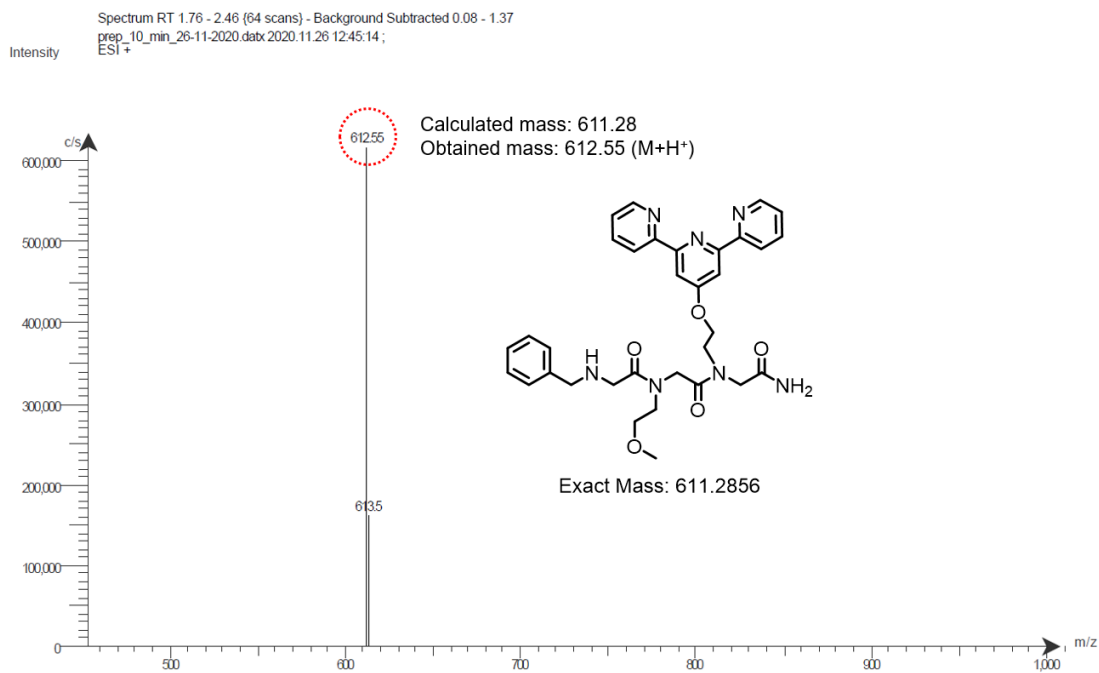


Figure S29. ESI-MS of peptoid **TPT-OCH₃** in water.

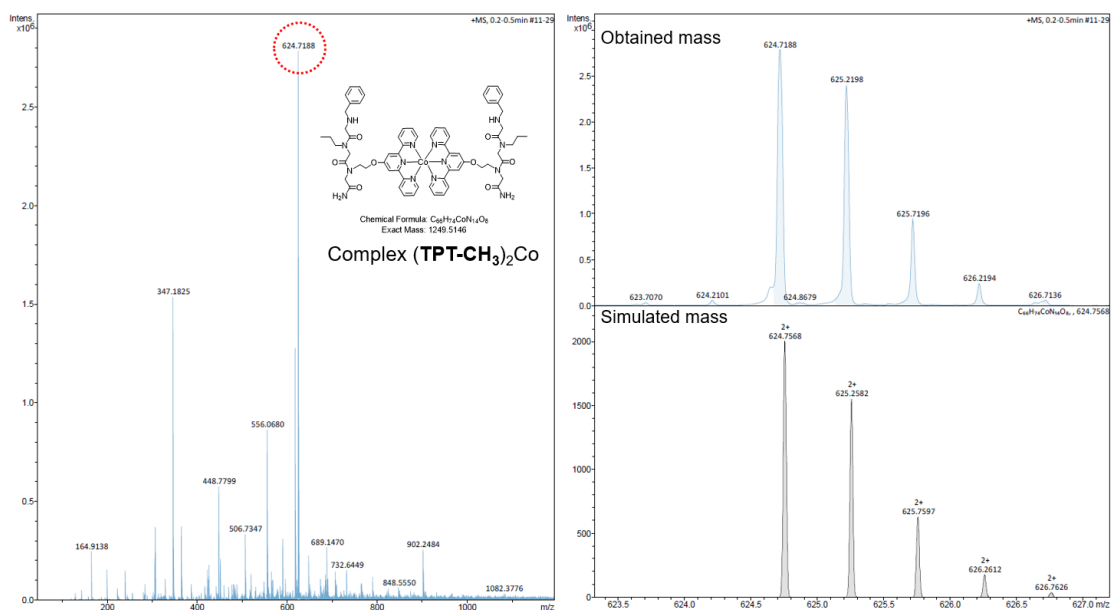


Figure S30. High-resolution ESI-MS of complex $(\text{TPT-CH}_3)_2\text{Co}$ in 0.1M phosphate buffer at pH 9.0.

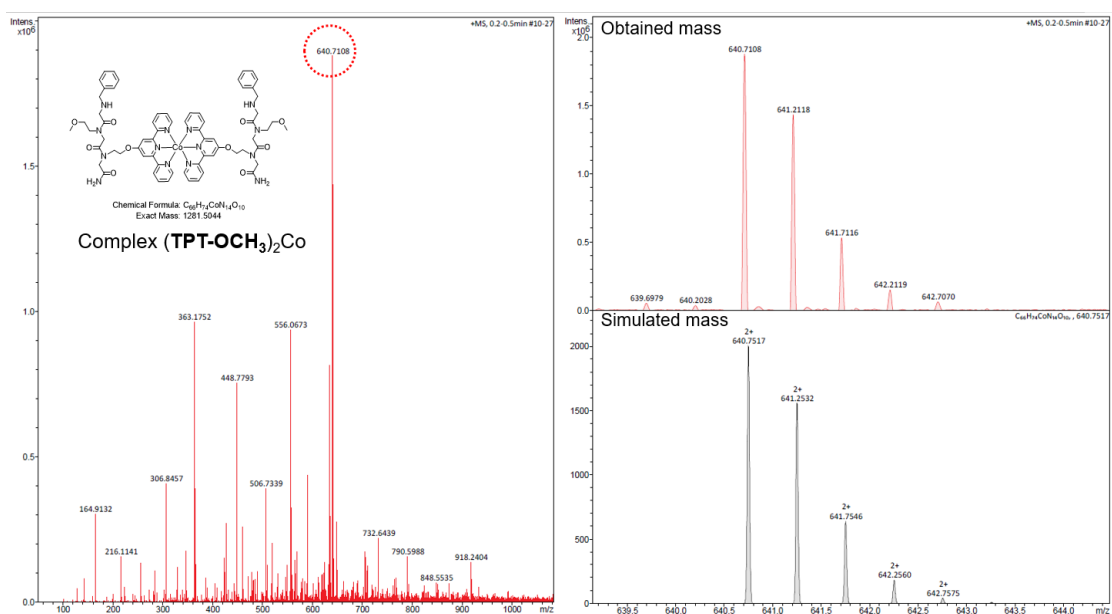


Figure S31. High-resolution ESI-MS of complex $(\text{TPT-OCH}_3)_2\text{Co}$ in 0.1M phosphate buffer at pH 9.0.

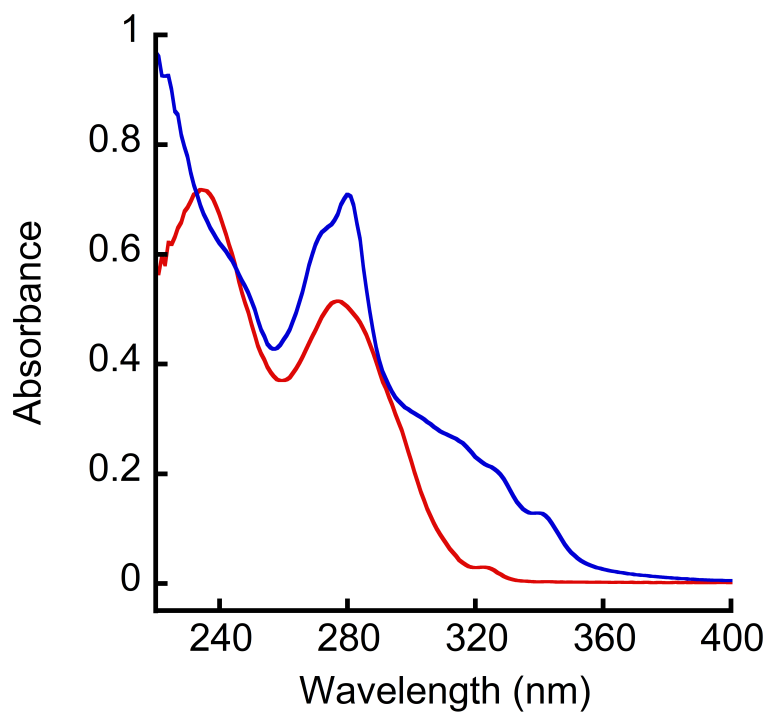


Figure S32. UV-Vis spectra of 49 μM of the peptoid **TPT-CH₃** (red line) and complex **(TPT-CH₃)₂Co** (blue line) in water.

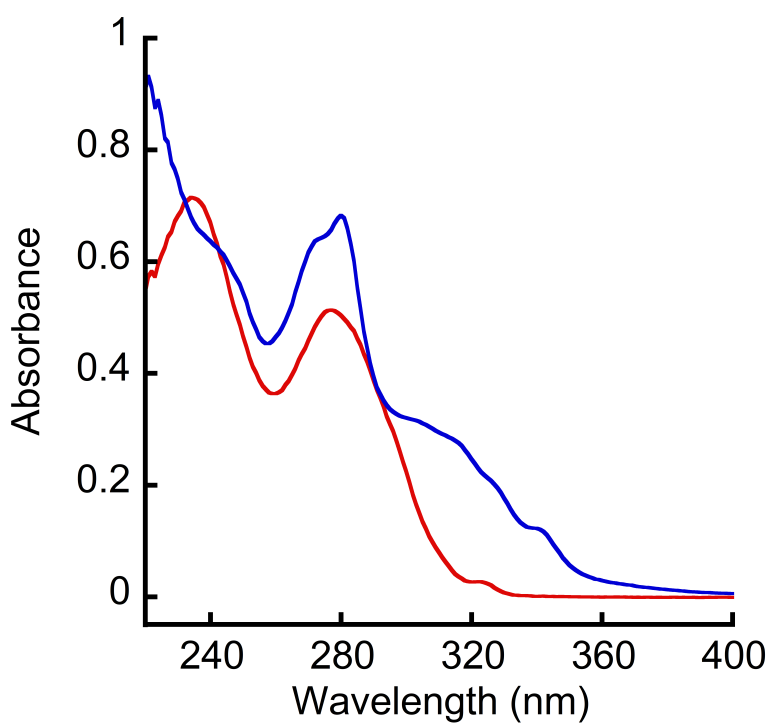


Figure S33. UV-Vis spectra of 49 μM of the peptoid **TPT-OCH₃** (red line) and complex **(TPT-OCH₃)₂Co** (blue line) in water.

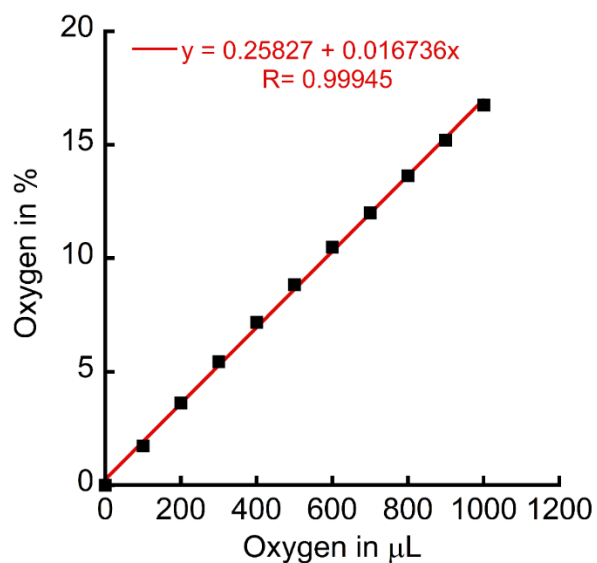
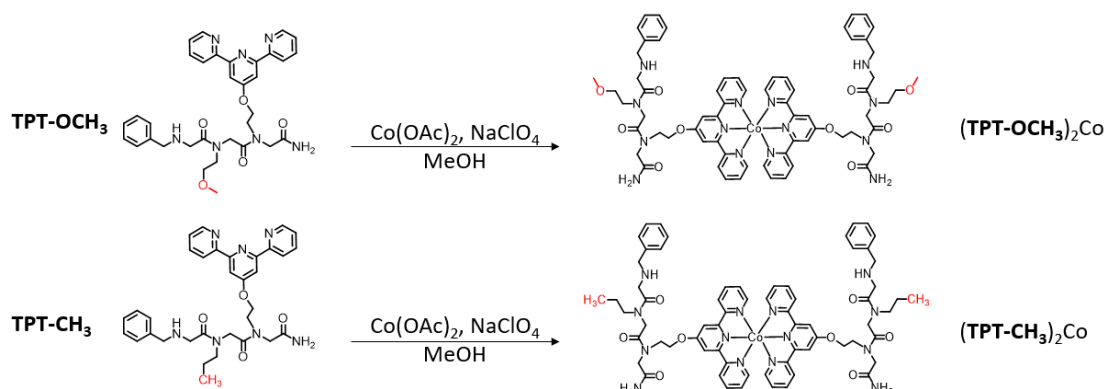


Figure S34. Plot of oxygen sensor calibration from % to μL unit.

Supplementary Schemes



Scheme S1. Molecular structures of peptoid TPT-OCH_3 and TPT-CH_3 , and corresponding Co complexes $(\text{TPT-OCH}_3)_2\text{Co}$ and $(\text{TPT-CH}_3)_2\text{Co}$ (the substituted groups are highlighted in red color), with the same complexation method as TPT_2Co .

Supplementary Equations

$$i_{cat} = n_{cat}FA[Co](k_{cat}D_{Co})^{1/2} \dots\dots(\text{eqn. S1})$$

- i_{cat} : the current intensity of catalytic peak at +1.46 V vs. NHE in A.
- n_{cat} : the number of electrons involved in water oxidation.
- A : active electrode surface area in cm^2 .
- F : Faraday constant in C/mol.
- $[Co]$: the concentration of catalyst TPT_2Co , mol/cm^3 .
- k_{cat} : the rate constant for water oxidation in s^{-1} (first-order).
- D_{Co} : the diffusion coefficient in cm^2/s .

$$i_d = 0.496(n_dF)^{3/2}A[Co]\left(\frac{\alpha D_{Co}v}{RT}\right)^{1/2} \dots\dots(\text{eqn. S2})^6$$

- i_d : the peak current of the non-catalytic peak at *ca.* +1.0 V vs. NHE.
- n_d : the number of electrons involved the oxidation.
- A : active electrode surface area in cm^2 .
- F : Faraday constant in C/mol.
- $[Co]$: the concentration of catalyst TPT_2Co , mol/cm^3 .
- α : transfer coefficient of the catalyst.
- D_{Co} : the diffusion coefficient in cm^2/s .
- v : scan rate in V/s.
- R : gas constant in J/K•mol.

$$\frac{i_{cat}}{i_d} = 1.827k_{cat}^{1/2}v^{-1/2} \dots\dots(\text{eqn. S3})$$

* eqn. S3 is the result of eqn. S1 is divided by eqn. S2.

$$FE\% = \frac{n_{O_2 \text{ oxygen sensor}}}{n_{O_2 \text{ theoretical}}} \times 100\% \dots\dots(\text{eqn. S4})$$

* eqn. S4 is the definition of Faradic efficiency (FE%) that the percentage of the contributed to the desired reaction, in this case is water oxidation.⁷

- $n_{O_2 \text{ oxygen sensor}}$: moles of oxygen obtained from the sensor.
- $n_{O_2 \text{ theoretical}}$: moles of oxygen calculated from accumulated charge.

$$FE\% = \frac{n_{O_2 \text{ oxygen sensor}}}{\frac{Q[C]}{n \cdot F}} \times 100\% \dots\dots \text{eqn. S5}$$

- Q : the coulomb of accumulated charge.
- n : the number of electrons involved in water oxidation.
- F : Faradaic constant in C/mol.

Supplementary Tables

Table S1. Data summary of Co-based electrocatalysts for homogeneous water oxidation in aqueous media from reported literature.

Catalyst	$E_{\text{onset}}^{\text{a}}$ – onset potential (vs. NHE)	$\eta_{\text{onset}}^{\text{b}}$ – onset overpotential (vs. NHE)	k_{cat} , s^{-1}	Buffer solution	pH	Ref.
TPT₂-Co^{III}	1.05 V	350 mV	108^d	0.1 M PBS^f	9.0	This work
[Co ^{II} (Py5)(OH ₂)]	/	/	79 ^d	0.1 M PBS	9.2	5
Co ^{III} H ^{βF} CX-CO ₂ H	1.45 V ^c	633 mV ^c	0.81 ^d	0.1 M PBS	7.0	8
[Co ^{III} (tpy)] ₂ (m-bpp) (m-1,2-O ₂)	1.82 V	714 mV	/	0.1 M PBS	2.1	9
Co ^{II} -TDMIImP	1.40 V ^c	583 mV ^c	1,400 ^d	0.2 M PBS	7.0	10
[(TPA)Co ^{III} -(μ-OH)(μ-O ₂)Co ^{III} (TPA)]	1.30 V	542 mV	~ 1.4 ^e	0.1 M BBS ^g	8.0	11
L ^{CH₂PO(OH)₂} -Co	1.27 V	453 mV	/	0.1 M PBS	7.0	12
[(L ₁ ⁴⁻)Co ^{III}]	1.20 V	383 mV ^c	7.53 ^d	0.1 M PBS	7.0	13
vitamin B ₁₂ (Co ^{III})	1.40 V ^c	783 mV ^c	/	0.1 M PBS	7.0	14
[Co ^{III} (dpaq)(Cl)]	1.24 V	482 mV	85 ^d	0.1 M PBS	8.0	15
Co ^{II} SO ₄	1.40 V	660 mV	87 ^d	0.1 M NaHCO ₃	8.3	16

a: all the reported onset potentials are approximate. b: $\eta = E_{\text{onset}} - (1.23 - 0.059 \times \text{pH})$. c: the parameters are calculated by + 0.20 V of the values vs. Ag/AgCl. d: calculated by Randles-Sevcik equation. e: measured by experiments. f: PBS = phosphate buffer solution. g: BBS = borate buffer solution.

References

1. G. Maayan, B. Yoo and K. Kirshenbaum, *Tetrahedron Lett*, 2009, **50**, 4297-4297.
2. T. W. Green and P. G. M. Wuts, *Protective Groups in Organic Synthesis*, Wiley-Interscience., 1999, 127-141, 708-711.
3. C. A. Kilner and M. A. Halcrow, *Dalton T*, 2010, **39**, 9008-9012.
4. L. J. Kershaw Cook, F. Tuna and M. A. Halcrow, *Dalton Trans.*, 2013, **42**, 2254-2265.
5. D. J. Wasylenko, C. Ganesamoorthy, J. Borau-Garcia and C. P. Berlinguette, *Chem Commun*, 2011, **47**, 4249-4251.
6. A. J. Bard and L. R. Faulkner, *Electrochemical methods: fundamentals and applications*, Wiley, New York, 2001.
7. S. M. Barnett, K. I. Goldberg and J. M. Mayer, *Nat Chem*, 2012, **4**, 498-502.
8. D. K. Dogutan, R. McGuire and D. G. Nocera, *J Am Chem Soc*, 2011, **133**, 9178-9180.
9. M. L. Rigsby, S. Mandal, W. Nam, L. C. Spencer, A. Llobet and S. S. Stahl, *Chem Sci*, 2012, **3**, 3058-3062.
10. D. Wang and J. T. Groves, *P Natl Acad Sci USA*, 2013, **110**, 15579-15584.
11. H. Y. Wang, E. Mijangos, S. Ott and A. Thapper, *Angew Chem Int Edit*, 2014, **53**, 14499-14502.
12. H. L. Sun, Y. Z. Han, H. T. Lei, M. X. Chen and R. Cao, *Chem Commun*, 2017, **53**, 6195-6198.
13. H. Y. Du, S. C. Chen, X. J. Su, L. Jiao and M. T. Zhang, *J Am Chem Soc*, 2018, **140**, 1557-1565.
14. H. M. Shahadat, H. A. Younus, N. Ahmad, S. G. Zhang, S. Zhuiykov and F. Verpoort, *Chem Commun*, 2020, **56**, 1968-1971.
15. S. Biswas, S. Bose, J. Debgupta, P. Das and A. N. Biswas, *Dalton T*, 2020, **49**, 7155-7165.
16. S. G. Patra, E. Illes, A. Mizrahi and D. Meyerstein, *Chem. Eur. J.*, 2020, **26**, 711-720.